

Transverse Thermoelectric Conductivity of Bilayer Graphene in Quantum Hall Regime

Chang-Ran Wang, Wen-Sen Lu, and Wei-Li Lee

Institute of Physics, Academia Sinica, Nankang, Taipei, Taiwan R.O.C.

(Dated: February 5, 2022)

Abstract

We performed electric and thermoelectric transport measurements of bilayer graphene in a magnetic field up to 15 Tesla. The transverse thermoelectric conductivity α_{xy} , determined from four transport coefficients, attains a peak value of $\alpha_{xy,\text{peak}}$ whenever chemical potential lies in the center of a Landau level. The temperature dependence of $\alpha_{xy,\text{peak}}$ is dictated by the disorder width W_L . For $k_B T/W_L \leq 0.2$, $\alpha_{xy,\text{peak}}$ is nominally linear in temperature, which gives $\alpha_{xy,\text{peak}}/T = 0.19 \pm 0.03 \text{ nA/K}^2$ independent of the magnetic field, temperature and Landau Level index. At $k_B T/W_L \geq 0.5$, $\alpha_{xy,\text{peak}}$ saturates to a value close to the predicted universal value of $4 \times (\ln 2) k_B e/h$ according to the theory of Girvin and Jonson. We remark that an anomaly is found in α_{xy} near the charge neutral point, similar to that in single-layer graphene.

PACS numbers: 65.80.Ck, 73.63.Bd, 72.15.Jf, 73.63.-b

Graphene, a single atomic layer of carbon sheet, has attracted considerable attention in the past few years [1]. Its unusual massless Dirac-fermion excitations, deriving solely from its honeycomb structure, have already unveiled many interesting transport phenomena [2–4]. More recently, there is a growing interest in the bilayer graphene partly due to the observation of tunable band gap by breaking inversion symmetry using external bias [5]. In addition, its chiral massive excitations are unique which give rise to the Berry phase 2π [6] and the two-fold orbital degeneracy in the zero-energy Landau level (LL). Several authors have pointed out that the coulomb exchange interaction within a LL with multi-degeneracy can break the symmetry and induce a spin-polarized quantum Hall state [7]. This becomes more pronounced in a bilayer graphene in which its zero-energy LL contains eightfold degeneracy (two spin, two valley and two orbital degeneracies) [8]. The lifting of spin degeneracy in the zero-energy LL has been uncovered in single-layer [9] and bilayer graphene [10] providing the evidence for exchange enhanced Zeeman splitting.

A fundamental issue in the quantum Hall effect (QHE) is the role of the edge current contribution to the observed quantized Hall conductivity in two dimensional electron system (2DES) with finite dimensions [11]. A current density \vec{J} generated by an electric field \vec{E} and a temperature gradient $(-\vec{\nabla}T)$ can be expressed by $\vec{J} = \vec{\sigma}\vec{E} + \vec{\alpha}(-\vec{\nabla}T)$, where $\vec{\sigma}$ and $\vec{\alpha}$ are the conductivity tensor and thermoelectric conductivity tensor, respectively. By assuming no transverse temperature gradient in the steady state, $\vec{\alpha}$ can be expressed in terms of conductivity σ_{xx} , Hall conductivity σ_{xy} , thermopower S_{xx} and Nernst signal S_{yx} as

$$\alpha_{xx} = \sigma_{xx}S_{xx} - \sigma_{xy}S_{yx} \text{ and } \alpha_{xy} = \sigma_{xy}S_{xx} + \sigma_{xx}S_{yx}. \quad (1)$$

We have used the definition of $S_{xx} \equiv -E_x/|\nabla T|$ (positive for hole) and $S_{yx} \equiv E_y/|\nabla T|$. Under an intense magnetic field, there exists current-carrying edge states within a magnetic length $\ell_B \equiv \sqrt{\hbar/(eB)}$ to the boundary. In the presence of \vec{E} , the induced difference in the edge currents at opposite sides due to the shift in chemical potential μ can be calculated to give $\delta I_{\text{edge}} = \nu e^2 V_H/h$, where ν is an integer and V_H is the Hall voltage. This agrees well with the observed quantized Hall conductivity $\sigma_H = \nu e^2/h$ with ν representing the filling factor. An alternative way to generate a non-zero δI_{edge} is to apply a $(-\vec{\nabla}T)$. The resulting δI_{edge} is also quantized, giving a universal value in the transverse thermoelectric tensor $\alpha_{xy} = (\ln 2)k_B e/h$ whenever μ sits at the center of a LL according to Girvin and Jonson's (GJ) theory [12, 13]. Recently, measurements on single-layer graphene [14] found that α_{xy}

is consistent with the predictions of GJ. In this work, we report electric and thermoelectric transport measurements in bilayer graphene. α_{xy} is determined from σ_{xx} , σ_{xy} , S_{xx} and S_{yx} . It reaches a peak value of $\alpha_{xy,peak}$ whenever μ crosses the center of a LL. The temperature and magnetic field dependences of $\alpha_{xy,peak}$ are then discussed and compared to the Mott relation [15].

Bilayer graphene samples were prepared by mechanical exfoliation from high quality bulk graphite on a doped silicon substrate, which serves as a bottom gate, with 300 nm of silicon dioxide. The number of layer was first identified from the optical contrast and then further confirmed by the pattern of σ_{xy} plateau in quantum Hall regime. The device shown in the inset of Fig. 2 was fabricated using electron beam lithography [14, 16, 17], comprising four electrodes, a local heater and two local thermometers, followed by Cr(1 nm)/Au(40 nm) film deposition and lift-off process. A $(-\vec{\nabla}T)$ across the bilayer graphene was modulated by feeding an alternating current to the local heater at a frequency $\omega \sim 3$ Hz. The thermoelectric signals S_{xx} and S_{yx} are then detected at second harmonic 2ω using a lock-in amplifier. Similarly, the temperature gradient is determined by feeding a direct current to the thermometer while detecting its resistance oscillation at 2ω . The $(-\vec{\nabla}T)$ we used is typically in a range from 10 mK/ μm to 50 mK/ μm . Both S_{xx} and S_{yx} signals are found to scale linearly with $(-\vec{\nabla}T)$ as expected. The results from two devices, labeled as S37 and S45 with different sample geometry, show consistent behavior which would be described in detail as follows.

Fig. 1 shows S_{xx} as a function of applied gate voltage V_g at different temperatures ranging from 15 K to 300 K in S37. S_{xx} equals zero at charge neutral point (CNP) ($V'_g \equiv V_g - V_{g0} = 0$, $V_{g0} = +5$ V) while its magnitude increases rapidly away from CNP and reaches a maximum value of S_m at $|V'_g| \approx +15$ V corresponding to a carrier density $n_c \approx 3 \times 10^{12} \text{cm}^{-2}$ determined from its Hall coefficient. S_{xx} monotonically increases with increasing temperature giving $|S_m| \approx 95 \mu\text{V}/\text{K}$ at 300 K. The upper-right inset of Fig. 1 plots the temperature dependence of $|S_m|$ and $|S_{xx}(V_g = 80\text{V})|$, in which $T^{1/2}$ and T , respectively, power law fittings shown as red lines agree well with the data points. On the other hand, $1/S_{xx}$ is practically linear with V_g away from CNP ($|V'_g| \geq 20$ V), which is shown at selected temperature of $T=300$ K, 120 K and 50 K in the lower-left inset of Fig. 1. From semi-classical theory for a free electron system, the thermopower can be described by $S_{xx} = -\pi^2/2(k_B/e)(k_B T/\epsilon_F)$, where ϵ is the Fermi energy. Since $\epsilon_F \propto k_F^2 \propto V'_g$ in a bilayer graphene, the observation of

$S_{xx} \propto T/V'_g$ away from CNP shown in the inset of Fig. 1 is then consistent with the free electron model. We also note that the $T^{1/2}$ dependence of S_m near CNP is different from the T-linear dependence found in single-layer graphene [14, 16]. As it turns out, the failure of the semi-classical theory near CNP persists to the quantum Hall regime.

As a standard practice, $\sigma_{xx}(\sigma_{xy})$ and $S_{xx}(S_{yx})$ under a field were (anti)symmetrized with respect to the magnetic field to exclude the contribution from mis-alignment of electrodes. At 15 Tesla, the observed Hall plateau of $\sigma_{xy} = \nu e^2/h$ in S45 (the upper panel in Fig. 2), where $\nu = \pm 4, \pm 8$ is the filling factor, indicates the onset of quantum Hall effect even at temperature up to 100 K. The $8e^2/h$ step in σ_{xy} across the CNP ($V_{g0} \simeq +29.4$ V) further confirms the bilayer graphene nature in S45, where its LL energy, given by $E_n = \hbar\omega_C\sqrt{N(N-1)}$ with the LL index N and cyclotron frequency $\omega_C = eB/m^*$, has two-fold orbital degeneracy ($N=0$ and 1) at zero-energy LL. Using $m^*=0.054m_e$ [8], the LL energy difference $\Delta E = E_2 - E_0 \simeq 530$ K. From low-field Hall measurement, we determined the mobility $\mu_c \simeq 2,600\text{cm}^2/\text{V-sec}$ in S45 and the gate capacitance $C_g \simeq 110 \text{ aF}/\mu\text{m}^2$. If naively using $E=(C_g/e)(\pi\hbar/2m^*)V'_g$, the LL spacing equals $\Delta E \simeq 560$ K, obtained from σ_{xx} peaks in Fig. 2, which is reasonably close to the theoretical value (530 K). Similarly, the disorder width W_L , defined as the full-width at half-maximum of the σ_{xx} peaks (lower panel in Fig. 2), gives ~ 180 K. Therefore, the criteria of $\Delta E \gg W_L, k_B T$ for quantum Hall regime is justified. We remark the appearance of double-peak feature in σ_{xx} with slanted σ_{xy} plateau near CNP, which suggests the lifting of spin degeneracy at zero-energy LL as pointed out recently by Zhao, *et al.* in a bilayer graphene [18]. The sheet resistance at CNP R_0 turns out to be nearly T independent below 30 K in zero field (the middle inset of Fig. 2). In contrast, the R_0 at 15 Tesla increases by 50% as T drops to 8 K, which basically agrees with previous reports of field-induced insulating state [18, 19].

Fig. 3 (a) shows V_g dependence of S_{xx} and S_{yx} in S37 at $\mu_0 H=15$ Tesla and $T=15$ K shown as thin black line and thick red line, respectively. The corresponding σ_{xx} (thin black line) and σ_{xy} (thick red line) vs. V_g are plotted in Fig. 3 (b) with N up to 4. A double Gaussian fit to the σ_{xx} near CNP shown in the thick blue line indicates an excess conductivity near CNP. Both S_{xx} and S_{yx} exhibit repeatable oscillations with V_g that effectively shifts the position of μ in bilayer graphene. When μ crosses the center of a LL, S_{xx} attains a peak value that progressively reduces in magnitude at higher N while S_{yx} , on the other hand, is nearly zero. Around CNP ($V_{g0} \simeq +5$ V), however, a large and broad peak of $S_{yx} \simeq +18\mu$

V/K is observed instead. Using Eq. 1, the obtained α_{xx} and α_{xy} as a function of V_g are shown in Fig. 3 (c). α_{xy} is positive and reaches a local maximum value of $\alpha_{xy,peak} \simeq 3 \text{ n A/K}$ for $N=0(1), 2, 3$ and 4 when μ crosses the center of a LL, while α_{xx} approaches zero instead. We also performed a current annealing ($j \sim 3 \times 10^8 \text{ A/cm}^2$) on S37, which causes the shift of V_{g0} from $+5 \text{ V}$ to -13 V as demonstrated by dashed lines in Fig. 3. Nevertheless, no other major variations in V_g dependence are found to result from the current annealing process.

In order to further explore the temperature dependence of α_{xy} , we performed measurements at different temperatures up to 100 K . At low temperatures and 15 Tesla , both α_{xy} and S_{yx} are practically linear in T as demonstrated in Fig.4 (a), where $\alpha_{xy}/T-V_g$ at $T=15 \text{ K}, 20 \text{ K}$ and 25 K all collapse onto a single curve, and so does $S_{yx}/T-V_g$. According to semi-classical theory (generalized Mott relation), α_{xy} and S_{yx} can be described by $\alpha_{xy} = \frac{\pi^2}{3} \frac{k_B^2}{e} T (\frac{\partial \sigma_{xy}}{\partial \varepsilon})_{\varepsilon=\mu}$ and $S_{yx} = \frac{\pi^2}{3} \frac{k_B^2}{e} T (\frac{\partial \tan \theta_H}{\partial \varepsilon})_{\varepsilon=\mu}$, where $\tan \theta_H \equiv \sigma_{xy}/\sigma_{xx}$ is the Hall angle. Therefore, we expect that $\alpha_{xy}/T \propto (\frac{\partial \sigma_{xy}}{\partial V_g})(\frac{\partial V_g}{\partial \varepsilon})_{\varepsilon=\mu}$. Similarly, $S_{yx}/T \propto (\frac{\partial \tan \theta_H}{\partial V_g})(\frac{\partial V_g}{\partial \varepsilon})_{\varepsilon=\mu}$. The calculated $\frac{\partial \sigma_{xy}}{\partial V_g}$ and $\frac{\partial \tan \theta_H}{\partial V_g}$ are shown as orange and green dashed lines, respectively, in Fig. 4 with arbitrary units, which qualitatively agree with the measured α_{xy}/T and S_{yx}/T except near the CNP. The term $(\frac{\partial V_g}{\partial \varepsilon})_{\varepsilon=\mu}$ is proportional to the density of state that gives minor influence to the behavior. We noticed the apparent electron-hole asymmetry in the magnitude of the calculated $\frac{\partial \sigma_{xy}}{\partial V_g}$ and $\frac{\partial \tan \theta_H}{\partial V_g}$, which may result from the shorting of voltage leads to the ‘‘hot-spot’’ near the current leads [20]. On the contrary, S_{xx} and S_{yx} , generated by a $(-\vec{\nabla}T)$ across bilayer graphene, exhibit much less asymmetry due to the hot-spot shorting effect. The deviation from the calculated value is evident near CNP and more dramatic in S_{yx} . The temperature dependence of $\alpha_{xy,peak}$ in S37 and S45 at 15 Tesla and $N=0(1), 2, 3$ and 4 are shown in Fig. 4 (b), where closed symbols and open symbols refer to the values in S37 and S45, respectively. Even though there is a minor variation in $\alpha_{xy,peak}$ at different N s and different samples, it basically follows T linear dependence below 30 K ($k_B T/W_L \simeq 0.2$). The corresponding values of $\alpha_{xy,peak}/T$ are plotted as a function of $\mu_0 H$ in the inset of Fig. 4 (b), averaged to a constant value of $\alpha_{xy,peak}/T = 0.19 \pm 0.03 \text{ nA/K}^2$ independent of $\mu_0 H$, N , and T . As T increases above 80 K ($k_B T/W_L \simeq 0.5$), it flattens up to a nearly constant value of $\alpha_{xy,peak} \simeq 8.5 \pm 1 \text{ nA/K}$, close to the universal value of $4 \times (\ln 2) k_B e/h$ (red thick line in Fig. 4).

The disorder width W_L , estimated to be $\sim 150 \text{ K}$ and $\sim 180 \text{ K}$ in S37 and S45, respectively, turns out to be an important parameter for the behavior of α_{xy} shown in Fig. 4 (b). At low

temperature $k_B T \ll W_L$, the number of disorder-induced extended states participating the diffusive transport increases with T , which gives rise to the T linear dependence in $\alpha_{xy,peak}$ similar to that in a ferromagnetic metal [21]. When $k_B T$ raises to a value comparable to W_L , further increment in T no longer includes more extended states. Therefore, $\alpha_{xy,peak}$ approaches the universal value of $4 \times (\ln 2) k_B e/h$. We do, however, observe a smaller $\alpha_{xy,peak}$ value ($\sim 18\%$ lower) at $N=0(1)$ near CNP. The broad peak of α_{xy} at $N=0(1)$ is in big contrast to the sharp and narrow peak observed in a single-layer graphene at similar field strength [14]. We attribute this to be the lifting of spin degeneracy in the bilayer graphene, inferred from the double peak feature in σ_{xx} that is attainable at lower field due to higher degeneracy at zero-energy LL [8]. A crude estimation of the spin splitting energy ΔE_{spin} from the double-peak in σ_{xx} at 15 Tesla gives $\Delta E_{spin} \simeq 26$ meV (~ 300 K) which is 15-fold larger than the regular Zeeman energy at the same field. In addition, the failure of Mott relation near CNP observed in bilayer graphene (Fig. 4 (a)) may result from the proposed novel phase of counter-propagating edge channels with opposite spin in spin-polarized quantum Hall regime [7]. We also remark that the behavior of α_{xy} is well reproduced in S37 and S45 with sample width to length aspect ratio of 1.3 and 2.4, respectively. Current annealing was found to cause insignificant influence except shifting the V_{g0} . The anomaly near CNP, arising either from an intrinsic effect of the chiral fermion or from an extrinsic effect such as electron-hole puddles [22], remains an open question. Further investigation in samples with higher mobility is required in order to resolve this issue.

In summary, we performed electric and thermoelectric transport measurements of bilayer graphene in quantum Hall regime. Double peak feature in σ_{xx} at $N=0(1)$ LL suggests the lifting of the spin degeneracy due to the possible exchange-enhanced Zeeman coupling. The disorder width W_L separates two different regimes for the behavior of $\alpha_{xy,peak}$. For $k_B T/W_L \leq 0.2$, $\alpha_{xy,peak}$ is practically linear in T , giving $\alpha_{xy,peak}/T = 0.19 \pm 0.03$ nA/K² independent of the magnetic field, temperature and LL index N . For $k_B T/W_L \geq 0.5$, $\alpha_{xy,peak}$ saturates to a value of $\alpha_{xy,peak} \simeq 8.5 \pm 1$ nA/K close to the predicted value of $4 \times (\ln 2) k_B e/h \simeq 9.24$ nA/K based on GJ theory of edge current model. We also found anomalous behaviors in S_{yx} and α_{xy} near CNP, where semi-classical theory does not provide satisfactory explanation. This may imply the existence of a novel phase of counter-propagating edge channels with opposite spin in spin-polarized quantum Hall regime, which may have potential application in spin-electronics.

The authors acknowledge the funding support from Nation Science Council in Taiwan and technical support from the Core Facilities for Nanoscience and Nanotechnology at Academia Sinica in Taiwan.

Note added.- During the preparation of this manuscript, we became aware of a related work at lower field (≤ 7 Tesla) by Nam et al. [23], which shows consistent result with our data.

-
- [1] K. S. Novoselov, A. K. Geim, S. V. Morozov, D. Jiang, M. I. Katsnelson, I. V. Grigorieva, S. V. Dubonos, and A. A. Firsov, *Nature* 438, 197 (2005);
 - [2] K. S. Novoselov, Z. Jiang, Y. Zhang, S. V. Morozov, H. L. Stormer, U. Zeitler, J. C. Maan, G. S. Boebinger, P. Kim, and A. K. Geim, *Science* 315, 1379 (2007).
 - [3] X. Du, I. Skachko, F. Duerr, A. Luican, and E. Y. Andrei, *Nature* 462, 192 (2009); K. I. Bolotin, F. Ghahari, M. D. Shulman, H. L. Stormer, and P. Kim, *Nature* 462, 196 (2009);
 - [4] M. I. Katsnelson, K. S. Novoselov, and A. K. Geim, *Nature Phys.* 2, 620 (2006); A F. Young and P Kim, *Nature Phys.* 5, 222 (2009).
 - [5] J. B. Oostinga, H. B. Heersche, X. Liu, A. F. Morpurgo, and L. M. K. Vandersypen, *Nature Mater.* 7, 151(2008); Y. Zhang, T. T. Tang, C. Girit, Z. Hao, M. C. Martin, A. Zettl, M. F. Crommie, Y. Ron Shen, and F. Wang, *Nature* 459, 820(2009).
 - [6] E McCann and V. I. Falco, *Phys. Rev. Lett.* 96, 086805 (2006); K. S. Novoselov, E. McCann, S. V. Morozov, V. I. Falco, M. I. Katsnelson, U. Zeitler, D. Jiang, F. Schedin, and A. K. Geim, *Nature Phys.* 2, 177 (2006).
 - [7] K. Nomura and A. H. MacDonald, *Phys. Rev. Lett.* 96, 256602 (2006); D. A. Abanin, K. S. Novoselov, U. Zeitler, P. A. Lee, A. K. Geim, and L. S. Levitov, *Phys. Rev. Lett.* 98, 196806 (2007).
 - [8] Y. Barlas, R. Cote, K. Nomura, and A. H. MacDonald, *Phys. Rev. Lett.* 101, 097601 (2008).
 - [9] Z. Jiang, Y. Zhang, H. L. Stormer, and P. Kim, *Phys. Rev. Lett.* 99, 106802 (2007).
 - [10] Y. Zhao, P. Cadden-Zimansky, Z. Jiang, and P. Kim, *Phys. Rev. Lett.* 104, 066801 (2010).
 - [11] B. I. Halperin, *Phys. Rev. B* 25, 2185 (1982); A. H. MacDonald and P. Streda, *Phys. Rev. B* 29, 1616 (1984).

- [12] S. M. Girvin and M. Jonson, *J. Phys. C: Solid State Phys.* 15, L1147 (1982).
- [13] L. Zhu, R. Ma, L. Sheng, M. Liu, and D. N. Sheng, *Phys. Rev. Lett.* 104, 076804 (2010).
- [14] J. G. Checkelsky and N. P. Ong, *Phys. Rev. B* 80, 081413R (2009).
- [15] M. Cutler and N. F. Mott, *Phys. Rev. B* 181, 1336 (1969).
- [16] P. Wei, W. Bao, Y. Pu, C. N. Lau, and J. Shi, *Phys. Rev. Lett.* 102, 166808 (2009).
- [17] Y. M. Zuev, W. Chang, and P. Kim, *Phys. Rev. Lett.* 102, 096807 (2009).
- [18] Y. Zhao, P. Cadden-Zimansky, Z. Jiang, and P. Kim, *Phys. Rev. Lett.* 104, 066801 (2010).
- [19] B. E. Feldman, J. Martin and A. Yacoby, *Nature Phys.* 5, 889 (2009).
- [20] J. Wakabayashi and S. Kawaji, *J. Phys. Soc. Jpn.* 44, 1839 (1978).
- [21] W. L. Lee, S. Watauchi, V. L. Miller, R. J. Cava, and N. P. Ong, *Phys. Rev. Lett.* 93, 226601 (2004).
- [22] E. H. Hwang, E. Rossi, and S. Das Sarma, *Phys. Rev. B* 80, 235415 (2009).
- [23] S. G. Nam, D. K. Ki, and H. J. Lee, arXiv:1005.4739

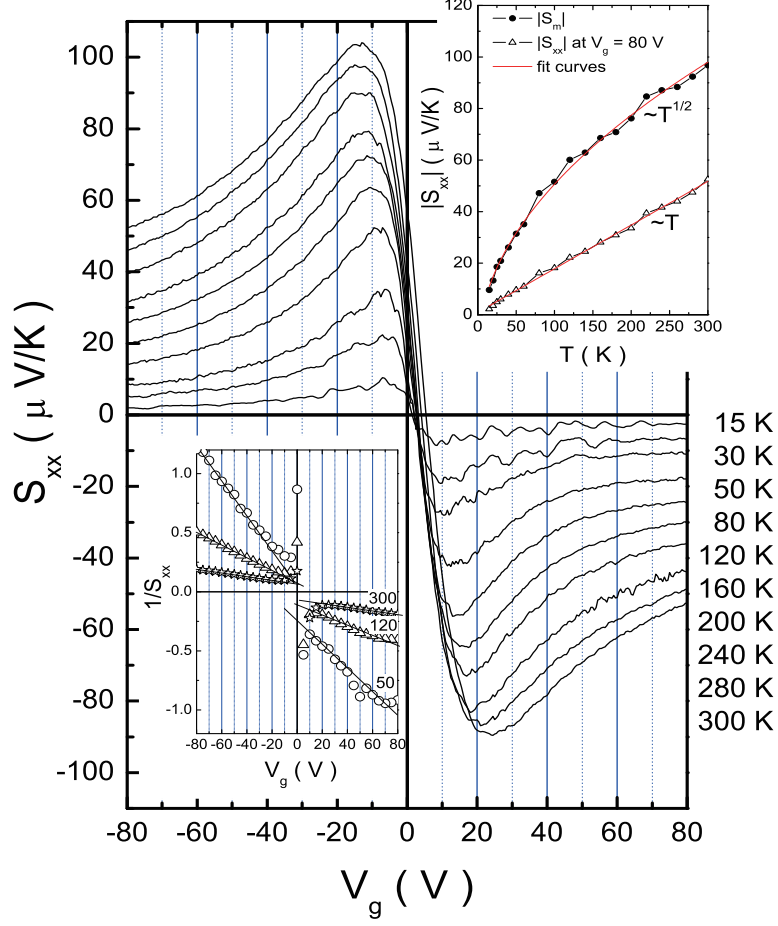


FIG. 1: Thermopower S_{xx} vs. V_g at temperatures ranging from 15 K to 300 K in S37. The upper-right inset shows the T dependence of maximum thermopower $|S_m|$ and $|S_{xx}|(V_g = 80\text{V})$. The red lines are the power law fitting to the data points. The lower-left inset plots $1/S_{xx}$ vs. V_g at selected temperatures.

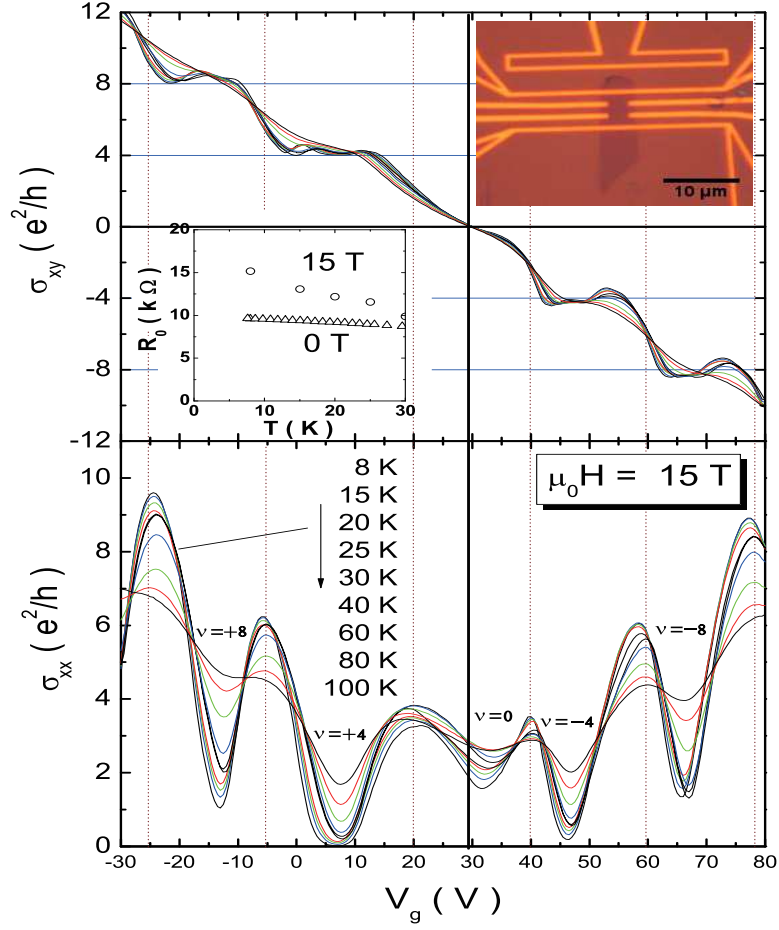


FIG. 2: V_g dependence of σ_{xy} and σ_{xx} at temperatures ranging from 8 K to 100 K in S45. An optical image of S45 is shown in the upper-right inset. The middle inset plots the sheet resistance at CNP R_0 vs. T at 15 Tesla (circle) and 0 Tesla (triangle).

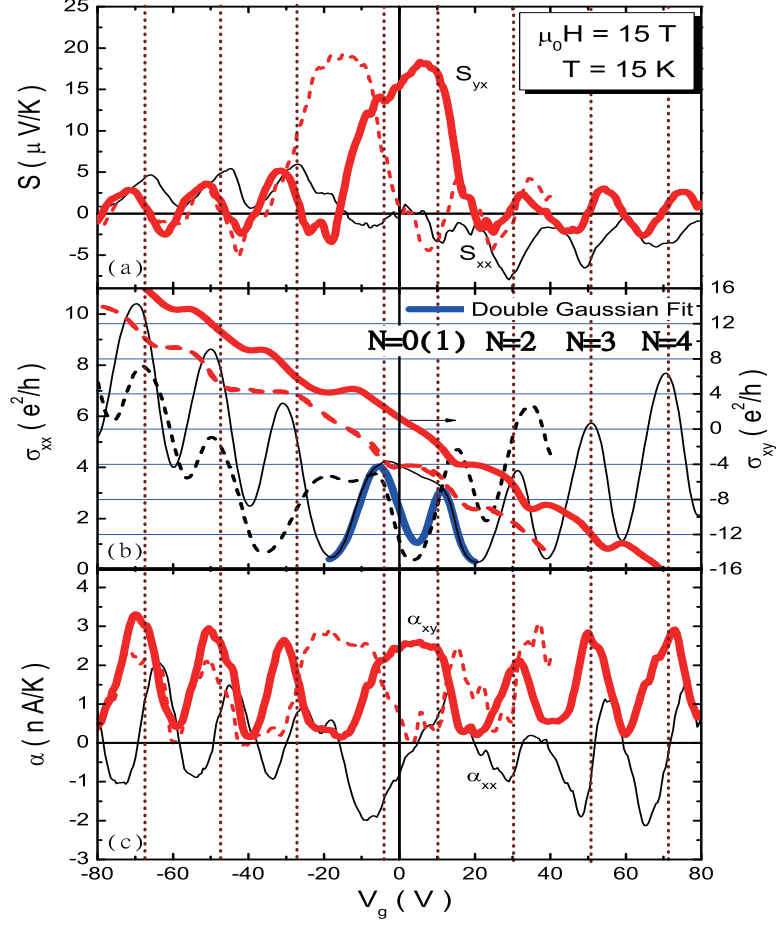


FIG. 3: V_g dependence of (a) S_{xx} and S_{yx} , (b) σ_{xx} and σ_{xy} and (c) α_{xx} and α_{xy} at 15 Tesla and $T=15$ K in S37. The dashed lines are the results from S37 after current annealing. The blue thick line is a double Gaussian fit to σ_{xx} near CNP.

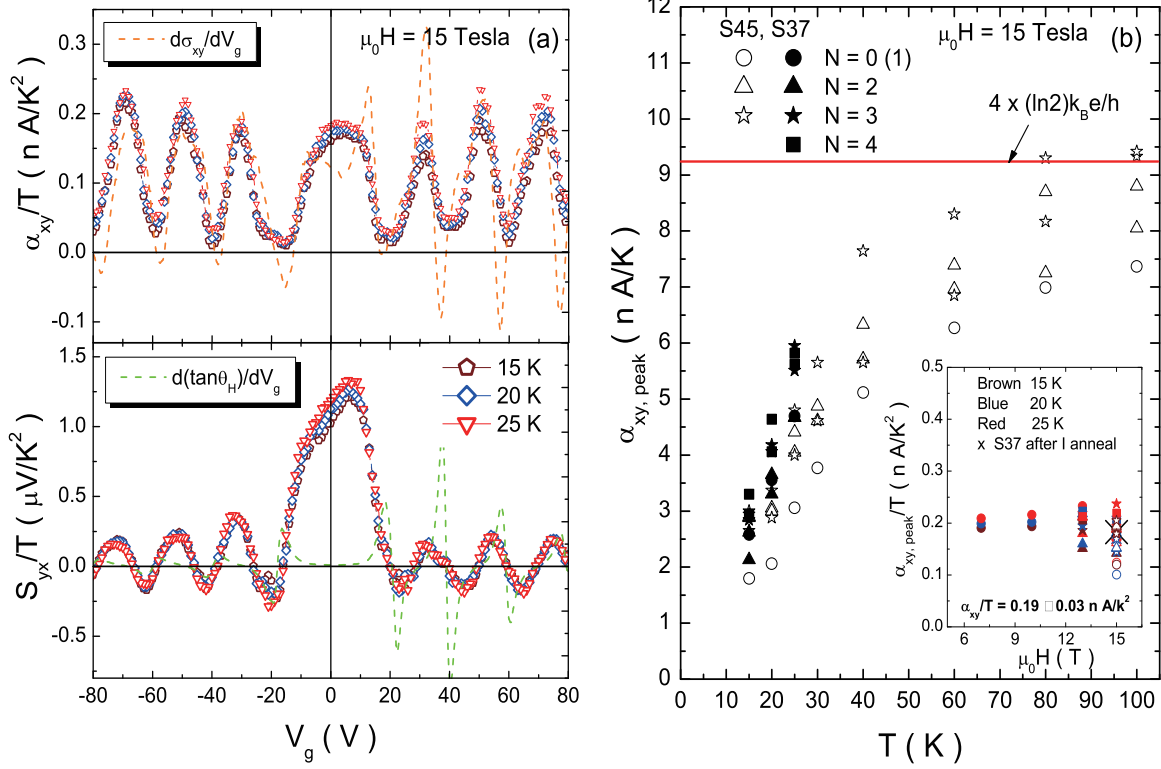


FIG. 4: (a) V_g dependence of α_{xy}/T (upper panel) and S_{yx}/T (lower panel) in S37 at 15 Tesla and three temperatures $T=15$ K (pentagon), 20 K (diamond) and 25 K (triangle). The orange (upper) and green (lower) dashed lines represent the Mott relation fits from $d\sigma_{xy}/dV_g$ and $d(\tan\theta_H)/dV_g$, respectively. (b) shows the T dependence of $\alpha_{xy,peak}$ in S37 (closed symbols) and S45 (open symbols) at 15 Tesla and different LLs $N=0(1)$ (circle), 2 (triangle), 3 (star) and 4 (square). The lower-right inset plots the $\alpha_{xy,peak}/T$ vs. $\mu_0 H$ with data points sharing the same symbols as (b).